Pergamon

Phys. Chem. Earth, Vol. 21, No. 4, pp. 225–230, 1996

0079-1946/96 $15.00 + 0.00

PII: S0079-1946(97)00039-6

Role of Stress Triggering in Earthquake Migration on the North Anatolian Fault

R. S. Stein[1], J. H. Dieterich[1] and A. A. Barka[2]

[1] U.S. Geological Survey, MS 977, Menlo Park, CA 94025, U.S.A.
[2] Istanbul Technical University, Department of Geology, Istanbul 80626, Turkey

Received 10 May 1996; accepted 3 March 1997

Abstract. Ten M≥6.7 earthquakes ruptured 1,000 km of the North Anatolian fault (Turkey) during 1939-92, providing an unsurpassed opportunity to study how one large shock sets up the next. Calculations of the change in Coulomb failure stress reveal that 9 out of 10 ruptures were brought closer to failure by the preceding shocks, typically by 5 bars, equivalent to 20 years of secular stressing. We translate the calculated stress changes into earthquake probabilities using an earthquake-nucleation constitutive relation, which includes both permanent and transient stress effects. For the typical 10-year period between triggering and subsequent rupturing shocks in the Anatolia sequence, the stress changes yield an average three-fold gain in the ensuing earthquake probability. Stress is now calculated to be high at several isolated sites along the fault. During the next 30 years, we estimate a 15% probability of a M≥6.7 earthquake east of the major eastern center of Erzincan, and a 12% probability for a large event south of the major western port city of Izmit. Such stress-based probability calculations may thus be useful to assess and update earthquake hazards elsewhere.

1 Introduction

New observations of the North Anatolian fault, as well as new methods to calculate how seismic stress transfer alters the probability of subsequent earthquakes, encourage us to study the 725-km-long 1939-44 sequence to investigate the conditions that promote progressive failure. Until recently, the fault geometry was poorly known, and there were few measurements of the 1939-44 earthquake fault slip (Ambraseys, 1970; Ketin, 1969), precluding calculation of the earthquake-induced stresses. Nor could the stress transferred by the steady or 'secular' stress accumulation be calculated, since the rate of deep fault slip driving the stress buildup was uncertain by a factor of four (Barka, 1992; Jackson & McKenzie, 1988; Le Pichon, *et al.*, 1993). New findings remove these obstacles: A threefold increase in measurements of earthquake slip, including a twelve-fold increase for the largest 1939 shock (Barka, 1996) provides data essential to model the earthquake stress changes (Fig. 1*b*). New detailed fault mapping (Barka, 1992; Saroglu & Kusçu, 1992) (Fig. 1*c*) reduces the uncertainty in the fault location from about ±25 km to ±5 km. Finally, geodetic analyses yield the slip rate along the fault (Oral, 1994; Straub & Kahle, 1994).

The North Anatolian fault emerges as a close analogue of the San Andreas fault in California, with the two continental transforms sharing similar slip rates, total length, and straightness relative to their poles of rotation (Fig. 1*a*). But while the San Andreas fault produced just two M≥6.7 earthquakes in this century (in 1906 and 1989), the North Anatolian fault has suffered ten such shocks, thus providing a superior natural laboratory to study earthquake interaction (Fig. 1*b-c*). We find that all but one earthquake increased the stress toward failure at the site of the subsequent shocks, and inhibited failure on most fault segments which did not rupture (Table 1). We argue that the calculated several-bar stress increases raised the earthquake probability during the ensuing decade three-fold, and we suggest why migrating earthquake sequences are so prevalent on the North Anatolian fault. Together with recent findings that aftershocks and background seismicity also concentrate where the stress has risen (Harris & Simpson, 1992; Harris, *et al.*, 1995; Jaumé & Sykes, 1992; King, *et al.*, 1994; Stein, *et al.*, 1994), these results offer a new approach to updatable forecasts of earthquake hazard.

2 Method

We calculate the static Coulomb stress changes on future fault planes in an elastic halfspace resulting from North Anatolian ruptures since 1939. Since we lack hypocentral depths for the Anatolian main shocks, we sample stress at 5 km intervals at a depth of 8 km, in the central part of the seismogenic crust. Failure is facilitated on a plane when the Coulomb failure stress σ_f rises $\sigma_f = \tau_\beta - \mu \sigma'_\beta$, where τ_β is the shear stress on the failure plane β (positive in the direction of fault slip) and σ_β' is the effective normal stress (positive in compression); $\mu\sigma'_\beta \approx \mu'\sigma_\beta$, where μ' is

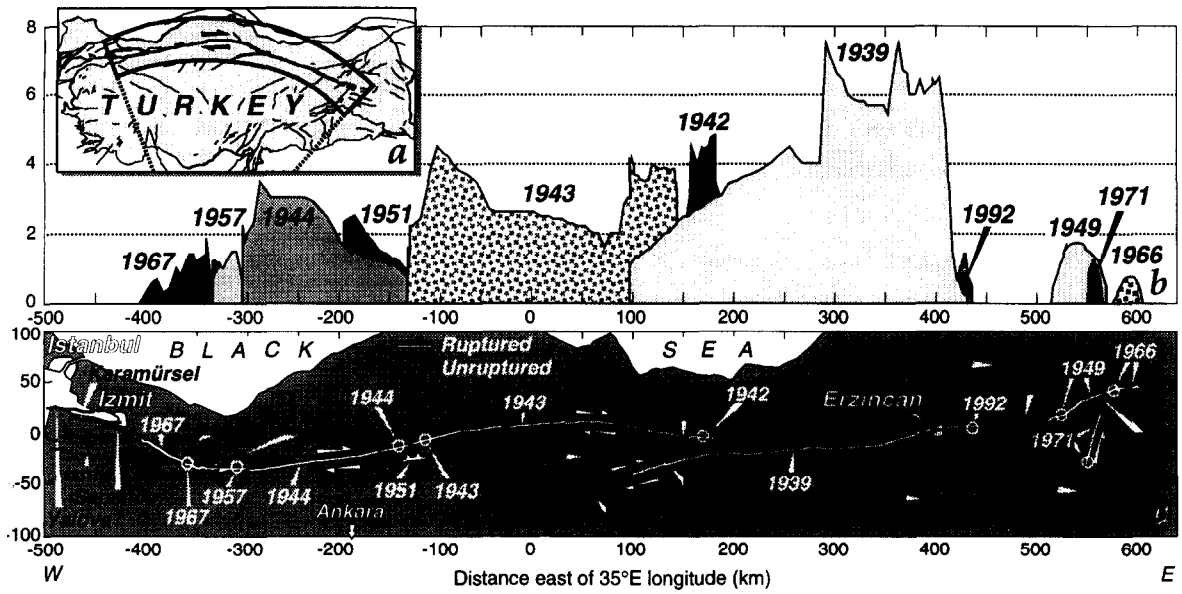

Fig. 1. (a) Active faults in Turkey (Barka, 1992; Saroglu & Kuşçu, 1992), with the North Anatolian fault in bold. GPS observations establish a 24±4 mm/yr (1s confid.) deep slip rate on the North Anatolian fault and reveal that the right-lateral transform describes a small circle about a (33.4±0.5°E, 31.1±1.3°N) Anatolia-Eurasia rotation pole, which lies at the intersection of the dashed bold lines (Oral, 1994). (b) Cumulative right-lateral slip associated with M≥6.7 earthquakes (Barka, 1995; Barka & Eyidogan, 1993; Bennett, et al., 1996). Slip in 1949, 1966, and 1971 is approximate. (c) The region inscribed by the solid red line in a is projected relative to the Anatolia-Eurasia rotation pole, so that a transform fault would strike due east-west; the North Anatolian fault is seen to deviate less than 40 km from being a simple right-lateral transform. Epicenters are circled.

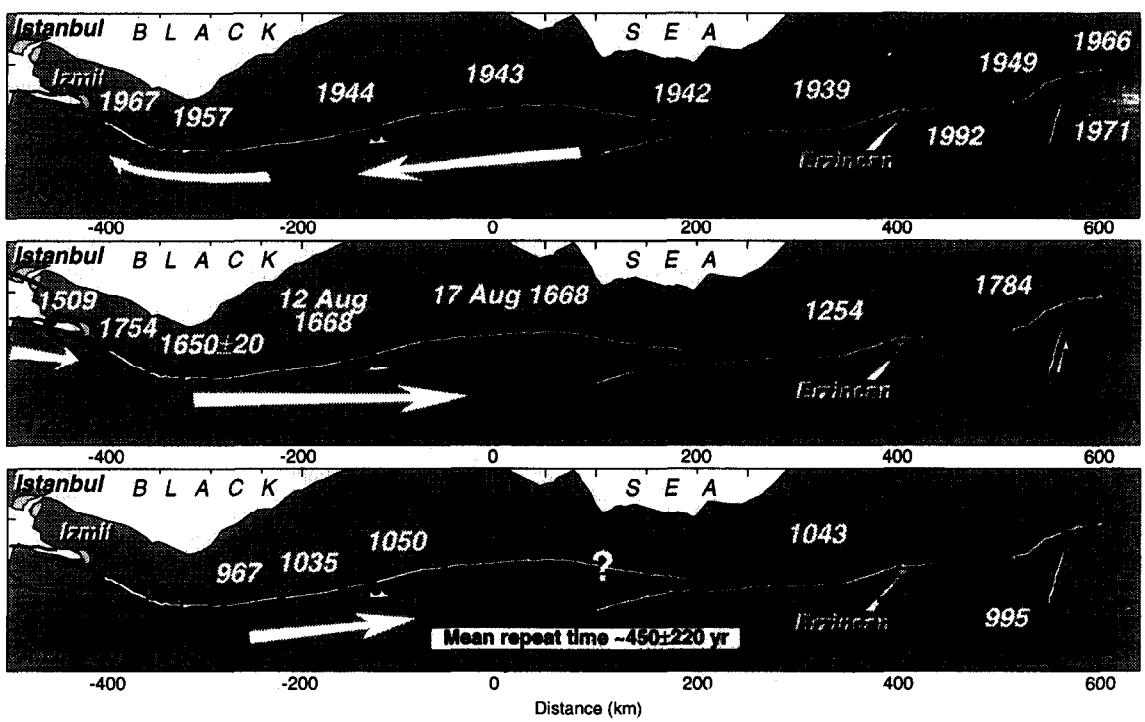

Fig. 2. Rupture zones for large historical earthquakes along the North and East Anatolian faults (Ambraseys & Finkel, 1988; Ambraseys & Finkel, 1995; Barka, 1992; Ikeda et al., 1991). Zones for earthquakes before 1939 are based largely on isoseismals, and are thus approximate. Earthquake progressions, indicated by arrows, occurred during three sequences but in different directions and rates.

the apparent coefficient of friction with range 0.0-0.75. The confining stress can be related to fluid pore pressure by Skempton's coefficient, B, the ratio of the change in pore pressure in a cavity to the change in applied stress, where $\mu' = \mu(1-B)$. We set μ'=0.4; equivalent to laboratory values of friction (μ~0.75) and moderate pore pressure if fluids are not fully expelled (B~0.5), or to a low value of friction as inferred for the San Andreas fault. A μ' of 0.4 also minimizes the calculation error caused by the uncertainty in μ' to ±25% (King, et al., 1994); compare, for example, *col. 2* (for $\mu' = 0.75$) and col. *3* (for $\mu' = 0.40$) in Table 2.

In addition to earthquakes, steady slip beneath the North Anatolia fault system transfers stress to the seismogenic portion of the fault. This we model with slip tapering from 0 at 12.5-km depth to the full rate below 24 km. GPS data give 24±4 mm/yr along the North Anatolian fault (Oral, 1994); near its western end, slip is partitioned with 16 mm/yr along the Karamürsel-Sapanca faults and 9 mm/yr along the Iznik-Geyve faults (Straub & Kahle, 1994). GPS data also resolve left-lateral slip of 18±6 mm/yr on the East Anatolian fault and ~5 mm/yr on the Northeast Anatolian fault (Bennett, *et al.*, 1996; Oral, 1994) (Fig. 1*c*). Stress builds in this model at 0.15 bar/yr along most of the North Anatolian fault. In addition, a uniform stress increase of 0.01 bar/yr is applied at all points to account for the small residual stressing associated with faults other than the North Anatolian system.

3 Results

Nine of 10 epicenters struck where the stress had been increased by the preceding earthquakes, typically by 3 bars (Table 2, *col. 3*). Similarly, 9 out of 10 shocks occurred where the mean stress over the entire future rupture had increased, typically by 2-4 bars (Table 2, *col. 4*). This calculation depends only on the fault slip, geometry, and μ'. The stress transfer averages about 10% of the stress released by the earthquakes (Table 1, *col. 6*), a substantial trigger. The 1942 shock lies in an off-fault lobe of stress increase resulting from the reverse slip along the Ezine segment in 1939 (Fig. 1c). The epicenter of the 1943 earthquake, which lies at the end of the rupture farthest from the 1942 shock, would appear to be at the wrong end of the 1943 rupture. However, the calculated stress change at the end of the 1943 rupture zone closest to the 1942 shock inhibited failure, and the epicenter of the 1943 shock lies within 40 km of where the stress change is most positive.

Most fault segments that sustained stress decreases have not ruptured, a further indication that stress changes influence earthquake occurrence. The typical stress change for the dozen unruptured segments since 1939 is -0.1 to -0.6 bars, in comparison with a 2- to 4-bar increase for those that have ruptured. Even when the secular stress accumulation during 1939-95 is included, the stress changes on the unruptured segments facilitated failure by only 1.2-1.6 bars, in comparison with a 3.6- to 6.1-bar increase for the segments that ruptured (Table 2, *col. 5*).

4 Earthquake probability Changes

The effect of the stress change on times of earthquake recurrence can be cast as a change in the probability of future events. The probability gain associated with the stress step is the probability after a stress increase divided by the probability prior to the step. The times of future earthquakes along a fault segment are uncertain because of intrinsic variability of the earthquake faulting process and uncertainty of the observations used to estimate recurrence time. Estimations of the probability of future events over a given time interval provide the means to account for these uncertainties. Departing from previous studies, we consider both permanent and transient effects of the stress changes on earthquake probabilities.

The permanent change in probability arises because increasing (or decreasing) the Coulomb stress on a fault segment shortens (or lengthens) the time required for continuing tectonic stressing to bring a segment to failure (Fig. 3*a-b*). Prior to the stress step, the probability for recurrence of an earthquake on a section of a fault, given an elapsed time t from the previous earthquake, is estimated following Working Group on California Earthquake Probabilities (1990). The effect of a stress increase on the conditional probability is to reduce the expected median recurrence time by the equivalent time required to accumulate the stress step $\Delta\sigma$ through the tectonic stressing process (Dieterich, 1988). To estimate probabilities, we require need values for the stressing rate, the earthquake repeat time and its standard deviation for $\mathbf{M} \geq 6.7$ earthquakes along the North Anatolia fault, as well as the time elapsed at the time of the 1939-67 sequence. The stressing rate in our model is 0.15 bar yr^{-1} along most of the North Anatolian fault system. Because the observations are sparse and uncertain, we do not distinguish different repeat times along the fault; instead we use the portions of the fault for which the record is longest to estimate a generic repeat time (Fig. 2). The historical record of earthquakes since about 990 A.D (Ambraseys, 1970; Ambraseys & Finkel, 1995; Ikeda, *et al.*, 1991) suggest a 450±220 yr repeat time, the time elapsed between the last events (in 1254-1668) to the 1939-67 sequence is thus taken to be ~425 yr (a weighted average).

A decaying effect of stress changes on earthqua probability arises from time-dependent earthquake nucleation deduced from laboratory observations of rate- and state-dependent fault constitutive behavior (Fig. 3*c*). The rate- and state-dependence of fault properties that give rise to time-dependent nucleation effects have been observed for a diverse variety of materials over the range of conditions for crustal earthquakes (Dieterich, 1988; Dieterich, 1994; Dieterich & Kilgore, 1996). Time-dependent nucleation strongly amplifies the background probability rate at the time of a sudden stress change,

followed by $1/t$ decay to the background rate (Fig. 3*c*). To evaluate the transient probability changes following a stress step, we treat earthquake occurrence as a non-stationary Poisson process. Integrating the solution of Dieterich (1994) for rate of activity following a stress change gives

$$N = r\left\{t + t_a \ln\left[\frac{1 + \left[\exp\left(\frac{-\Delta\sigma_f}{A\sigma}\right) - 1\right]\exp\left(\frac{-t}{t_a}\right)}{\exp\left(\frac{-t}{t_a}\right)}\right]\right\} \quad (1)$$

where N is the average expected number of events in the time interval, t is defined here as the time following the stress step, r is the average permanent probability rate following the stress step, in the interval $(0, t)$; t_a is the characteristic duration of the transient effect; and $\Delta\sigma_f$ is the calculated Coulomb stress change. A is a dimensionless fault constitutive parameter and σ is the effective normal stress. Since t_a and $A\sigma$ are unknown for the Anatolia sequence, we set t_a = 10.2 yr, the value derived for the Harvard CMT global catalog for M>5 at depths <70 km, and $A\sigma$ = 1 bar from analyses of aftershocks and foreshocks (Dieterich, 1994).

We give the probability gains in Table 3 for the transient and permanent gain, divided by the conditional probability for occurrence of an earthquake in the absence of a stress step. Here, the background permanent probability is about 3.6% per decade at any one M=6.7 segment along the fault. We find an average three-fold gain in the probability of an M≥6.7 earthquake during the decade after each triggering event, with a range of 1-19. After 1939, M≥6.7 earthquakes occurred at a rate more than three times higher than during the preceding half-century, in rough accord with the model.

5 Limitations of the Analysis

Although we incorporate stress changes caused by earthquakes and secular fault slip, we make several assumptions that influence our results. Because we use earthquake slip measured at the surface, we may underestimate the net slip at depth, and thus the stress change, by as much as 50%. Our assumed 12.5-km depth of coseismic slip is consistent with the 1992 Erzincan earthquake (Barka & Eyidogan, 1993; Bennett, et al., 1996), but it is unknown for the preceding events. The deep slip rate used for the secular model is also uncertain by ±8 mm/yr (95% confidence) (Oral, 1994). In addition, we neglect two time-dependent effects: Pore-fluid flow could raise μ' with time (Harris & Simpson, 1992; Jaumé & Sykes, 1992; Scholz, 1990), which would increase the stress changes by up to 25% (Table 2, *col. 2*). Postseismic asthenospheric relaxation transfers stress to the upper crust after an earthquake. An 12.5-km-thick elastic plate overlying an inviscid fluid approximates complete relaxation of the lower crust; this yields stresses twice as high and twice as broad as those calculated here (Stein, *et al.*, 1992). Thus most processes we omit would, if included, increase the calculated stress transfer. Several assumptions introduce uncertainty into our probability calculations. To estimate the permanent stress effects, we used a common repeat and elapsed time for large earthquakes on the Anatolian fault, whereas repeat times for the better studied San Andreas fault, for example, differ by almost a factor of two between the northern and southern segments. For the transient effects, we relied upon global average values for parameters where we lacked local information for Anatolia; these could vary by ±50%. Our analysis is least successful in explaining the occurrence of the 1943 earthquake, and the absence of a Yedisu segment earthquake. Nor do we account for the time lag between individual triggers and ruptures, which varied from months to decades.

6 Conclusions

We identify several faults with an heightened probability of failure. The port city of Izmit is most vulnerable to an earthquake on the Sapanca fault (Fig. 1*c*). Stress increases of 1.3-2.5 bars are found for the Geyve and Sapanca faults, which pose the greatest threat to Istanbul, particularly if the faults ruptured from east to west. The Sapanca fault last ruptured in 1878. We calculate a 30-yr probability during 1996-2026 for M≥6.7 shocks on the Geyve and Sapanca fault segments to be 12%; this is 7% higher than the rate before the these segments were stressed by the 1967 earthquake. The Yedisu (last rupture in 1784), Ovacik, and Göynük (last event in 1866) faults near Erzincan have been stressed toward failure by 1.7-9.2 bars. Erzincan, badly damaged during the 1939 and 1992 earthquakes, would be most affected if these faults ruptured toward the city (Fig. 1*c*). We calculate a 30-yr probability during 1996-2026 for M≥6.7 shocks on the Yedisu segment to be 15%; this value is 35% higher than the rate before the these segments were stressed by the 1992 Erzincan earthquake.

We find that earthquake-induced stress increases several bars promoted the North Anatolia earthquake sequence, each shock raising the probability of future earthquakes at the site of the next to strike. Clustering of strong shocks is the outstanding feature of seismicity over historical (Kagan & Jackson, 1991) and paleoseismic (Wallace, 1987) time periods, implying that the prospect of a large earthquake rises after a large event. Stress transfer offers a physical explanation for earthquake clustering and migration: stress drops on the slipped fault but rises at other sites nearby, bringing faults in these regions closer to failure. Coulomb stress calculations thus capture the most salient feature of earthquake distributions, and gives insight as to where the next event is more likely to strike.

Acknowledgments. This is an abbreviated version of Stein et al. (1997). We thank Pascal Bernard and Nicholas Ambraseys for reviews, and the Istituto Nazionale di Geofiscia for financial assistance.

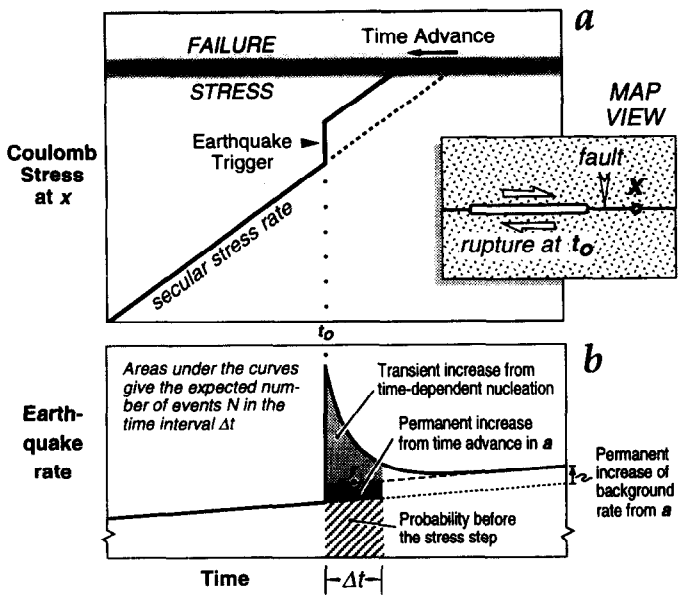

Fig. 3. Schematic illustration of a sudden stress increase Dsf on a fault at point x near an earthquake rupture at time to (inset). (a) The stress increase advances the time to the next rupture. If the stress were closer to failure at the time of the stress step, the trigger might have triggered an earthquake immediately. (b) The associated short-term (transient) and long-term (permanent) probability gain (Dieterich & Kilgore, 1996). The transient gain (curved portion of solid line) scales with the rate of aftershock decay, and the permanent gain (dashed to solid line) is typically a factor of 1.12 higher than the probability before the triggers the Anatolian sequence.

TABLE 1 Earthquake parameters and stress transfer

Earthquake Year	Date	Moment mag. M	M_o ** (10^{26} dyn-cm)	Mean Δτ* (bar)	Stress trigger‡ (bar)	Trigger ratio§ (%)	Time advance (yr)¶
1939	26 Dec	7.9	52.0	60	--	--	--
1942	20 Dec	6.9	1.7	42	4.7	11	8.4
1943	26 Nov	7.7	29.0	48	0.6	1	0.0
1944	01 Feb	7.5	15.0	34	5.8	17	31.4
1949	17 Aug	7.1	3.5	40	1.3	3	2.1
1951	13 Aug	6.8	1.4	25	1.7	7	11.0
1957	26 May	6.8	1.4	22	5.4	25	28.6
1966	19 Aug	6.6	0.6	15	8.2	55	30.0
1967	22 Jul	7.0	2.7	18	4.4	24	12.3
1971	22 May	6.8	1.2	11	3.5	32	4.6
1992	13 Mar	6.5	0.4	27	16.0	59	125.0
Average (all values)				*31*	*5.2*	*24*	*25.3*
Average (min/max excluded)				*34*	*4.4*	*22*	*18.1*

** Seismic moment calculated from surface slip (Fig. 1), assuming a 0 to 12.5-km width of faulting, and a shear modulus *G* of 3.15 x 10^{11} dyne-cm^{-2}.

* Mean static shear stress drop of all 5-km-long rupture patches.

‡ Mean earthquake-induced plus secular stress change along future ruptures.

§ Stress trigger (*col. 6*) divided by succeeding earthquake stress drop (*col. 5*).

¶ Mean earthquake-induced stress change (for μ=0.4) along the future rupture zone divided by the modeled secular stressing rate along that rupture.

Three modes to weigh the effect of the stress changes at the sites of future earthquakes. The trigger ratio is the Coulomb stress increase divided by the subsequent earthquake stress drop (*col. 6/col. 5*); the time advance gives the Coulomb stress increase divided by the local secular stressing rate.

TABLE 2 Stress transfer to future ruptures

	Coulomb failure stress change (bars)				
	Earthquakes only			Earthq.+secular	
Triggered Event	Epicentre μ'=0.75	Epicentre μ'=0.4	Mean μ'=0.4	Epicentre μ'=0.4	Mean μ'=0.4
1942	11.75	4.63	1.3	4.7	1.5
1943	0.00	0.01	-0.0	0.6	0.6
1944	6.56	6.39	4.8	7.3	5.6
1949	0.61	0.53	0.3	1.3	1.4
1951	1.49	1.71	1.7	1.7	1.7
1957	3.47	3.45	4.0	5.4	5.9
1966	3.85	4.03	3.0	8.2	5.4
1967	1.70	1.47	1.4	4.4	4.3
1971	0.71	0.58	0.5	3.5	3.2
1992	9.60	8.00	19.0	16.0	31.6
Average min/max excluded	*4.0*	*3.1*	*3.7*	*5.2*	*6.1*
	3.5	*2.9*	*2.0*	*4.4*	*3.6*

Cumulative stress transferred by M≥6.7 earthquakes and by secular stress accumulation since 1939, resolved onto future ruptures at 8 km depth. Faults were digitized at 5-km increments, with calculations performed with the fault projected in UTM coordinates, as in Fig. 1*a*. The stress change shown for the 1942 earthquake assumes that the Ezine fault (Fig. 1*c*) has a 50°-N dip and a 1:1 right-reverse-slip component (if the Ezine is treated as a vertical strike-slip fault, the mean change on the 1942 rupture zone is -6.0 bars and the epicentral change is -3.0 bars). The stress transferred by the 1951 earthquake is calculated for the 60°N-dipping Kursunlu thrust fault (Pinar, 1953), although the epicenter could lie on the North Anatolian fault. The epicentral stress for μ'=0.75 gives results for low pore fluid pressure.

TABLE 3 Triggered earthquake probabilities (450±220 yr repeat time)

Triggered Shock Year	Date	Probability before the stress step: Poisson	Conditional †	recurrence* time change (yr)	Conditional probability after the stress step‡: Permanent effect	Transient + perm. effect	Probability gain (col. 7÷ col. 4)
1942	20 Dec	0.022	0.036	-8.4	0.038	0.074	2.0
1943	26 Nov	0.022	0.036	0.0	0.036	0.036	1.0
1944	1 Feb	0.022	0.036	-31.4	0.041	0.204	5.6
1949	17 Aug	0.022	0.036	-2.1	0.037	0.044	1.2
1951	13 Aug	0.022	0.036	-11.0	0.038	0.087	2.4
1957	26 May	0.022	0.036	-28.6	0.041	0.174	4.8
1966	19 Aug	0.022	0.036	-30.0	0.041	0.140	3.9
1967	22 Jul	0.022	0.036	-12.3	0.038	0.078	2.1
1971	22 May	0.022	0.036	-4.6	0.037	0.050	1.4
1992	13 Mar	0.022	0.036	-125.0	0.059	0.704	19.4
Average				*-25.3*	*0.041*	*0.159*	*4.9*
Average (min/max values excluded)				*-16.1*	*0.039*	*0.105*	*2.9*

† Elapsed time is assumed to be 425 yr (weighted average time since complete rupture of the North Anatolian fault in earthquakes during 1254 and 1668; see Fig. 2).

* From eq (1), using the stress transfer in Table 2 (*col. 4*) divided by the secular stressing rate for each rupture zone (0.10-0.15 bar/yr).

‡ This uses the stress-modified recurrence time to compute the conditional probability for the ten years after the stress step.

References

Ambraseys, N. N., Some characteristic features of the Anatolian fault zone, *Tectonophysics*, **9**, 143-165, 1970.

Ambraseys, N. N., and C. F. Finkel, *The Seismicity of Turkey and Adjacent Areas: A historical review, 1500-1800*. Istanbul: Muhittin Salih EREN, 1995.

Barka, A., Slip distribution along the rupture zones of the 1939-1967 large earthquake migration in the North Anatolian fault, *Bull. Seismol. Soc. Am.*, in press, 1996.

Barka, A., and H. Eyidogan, The Erzincan earthquake of 13 March 1992 in eastern Turkey, *Terra Nova*, **5**, 190-194, 1993.

Barka, A. A., The North Anatolian fault zone, *Annales Tectonicae*, **VI** suppl., 164-195, 1992.

Bennett, R., R. Reilinger, and A. Barka, Coseismic displacement of the 1992 Erzincan earthquake, Eastern Turkey, from GPS observations, in prep., 1996.

Dieterich, J., A constitutive law for rate of earthquake production and its application to earthquake clustering, *J. Geophys. Res.*, **99**, 2601-2618, 1994.

Dieterich, J. H., Probability of earthquake recurrence with nonuniform stress rates and time-dependent failure, , **126**, 589-617, 1988.

Dieterich, J. H., and B. Kilgore, Implications of fault constitutive properties for earthquake prediction, *Proc. Nat. Acad. of Sci.*, in press, 1996.

Harris, R. A., and R. W. Simpson, Changes in static stress on southern California faults after the 1992 Landers earthquake, *Nature*, **360**, 251-254, 1992.

Harris, R. A., and R. W. Simpson, In the shadow of 1857—Effect of the great Ft. Tejon earthquake on subsequent earthquakes in southern California, *Geophys. Res. Letts.*, **23**, 229-232, 1996.

Harris, R. A., R. W. Simpson, and P. A. Reasenberg, Influence of static stress changes on earthquake locations in southern California, *Nature*, **375**, 221-224, 1995.

Ikeda, Y., Y. Suzuki, E. Herece, F. Saroglu, A. M. Isikara, and Y. Honkura, Geological evidence for the last two faulting events on the North Anatolian fault zone in the Mudurnu Valley, western Turkey, *Tectonophysics*, **193**, 335-345, 1991.

Jackson, J., and D. McKenzie, The relationship between plate motions and seismic moment tensors, and the rates of active deformation in the Mediterranean and Middle East, *Geophys. J. Int.*, **93**, 45-73, 1988.

Jaumé, S. C., and L. R. Sykes, Change in the state of stress on the southern San Andreas fault resulting from the California earthquake sequence of April to June 1992, *Science*, **258**, 1325-1328, 1992.

Kagan, Y. Y., and D. D. Jackson, Long-term earthquake clustering, *Geophys. J. Int.*, **104**, 117-133, 1991.

Ketin, I., Uber die nordanatolische Horizontalverschiebung, *Bull. Min. Res. Explor. Inst. Turkey*, **72**, 1-28, 1969.

King, G. C. P., R. S. Stein, and J. Lin, Static stress changes and the triggering of earthquakes, *Bull. Seismol. Soc. Amer.*, **84**, 935-953, 1994.

Le Pichon, X., N. Chamot-Rooke, P. Huchon, and P. Luxey, Implications des nouvelles mesures de géodésie spatiale en Grèce et en Turquie sur l'extrusion latérale de l'Anatolie et de l'Egée, *C. R. Acad. Sci. Paris*, **t. 316, Série II**, 983-990, 1993.

Oral, M. B. (1994) *Global Positioning System (GPS) Measurements in Turkey (1988-1992): Kinematics of the Africa-Arabia-Eurasia Plate Collision Zone*,. Ph.D. thesis, 344 pp., Mass. Inst. Tech.

Richter, C. F., *Elementary Seismology*. San Francisco: W.H. Freeman & Co., 1958.

Saroglu, F., and I. Kusçu, Active Fault Map of Turkey (1:1,000,000), In Ankara: Gen. Dir. of Mineral Res. & Explor. (MTA).

Scholz, C. H., *The Mechanics of Earthquakes and Faulting*. Cambridge: Cambridge University Press, 1990.

Sengor, A. M. C., N. Gorur, and F. Saroglu, Strike-slip faulting and related basin formation in zones of tectonic escape: Turkey as a case study, In K. T. Biddke & N. Christie-Blick (Eds.), *Strike-slip Faulting and Basin Formation* (pp. 227-264). Soc. Econ. Paleont. Min. Spec. Publ., 1985.

Stein, R. S., G. C. P. King, and J. Lin, Change in failure stress on the southern San Andreas fault system caused by the 1992 Magnitude=7.4 Landers earthquake, *Science*, **258**, 1328-1332, 1992.

Stein, R. S., G. C. P. King, and J. Lin, Stress triggering of the 1994 M=6.7 Northridge, California, earthquake by its predecessors, *Science*, **265**, 1432-1435, 1994.

Stein, R. S., A. A. Barka, and J. H. Dieterich, Progressive failure on the North Anatolian fault since 1939 by earthquake stress triggering, *Geophys. J. Int.*, **128**, in press, 1997.

Straub, C., and H.-G. Kahle, Global Positioning System (GPS) estimates of crustal deformation in the Marmara Sea region, Northwestern Anatolia, *Earth & Planet. Sci. Letts.*, **121**, 495-502, 1994.

Wallace, R. E., Grouping and migration of surface faulting and variations in slip rates on faults in the Great Basin province, *Bull. Seismol. Soc. Amer.*, **77**, 868-876, 1987.

Working Group on California Earthquake Probabilities, Probabilities of large earthquakes in the San Francisco Bay region, California, *U.S. Geol. Surv. Circular 1053*, 1990.